



HAL
open science

Valveless pumping at low Reynolds numbers

Gabriel Amselem, Christophe Clanet, Michael Benzaquen

► **To cite this version:**

Gabriel Amselem, Christophe Clanet, Michael Benzaquen. Valveless pumping at low Reynolds numbers. *Physical Review Applied*, 2023, 19 (2). hal-03797320

HAL Id: hal-03797320

<https://hal.science/hal-03797320>

Submitted on 4 Oct 2022

HAL is a multi-disciplinary open access archive for the deposit and dissemination of scientific research documents, whether they are published or not. The documents may come from teaching and research institutions in France or abroad, or from public or private research centers.

L'archive ouverte pluridisciplinaire **HAL**, est destinée au dépôt et à la diffusion de documents scientifiques de niveau recherche, publiés ou non, émanant des établissements d'enseignement et de recherche français ou étrangers, des laboratoires publics ou privés.

Valveless pumping at low Reynolds numbers

Gabriel Amselem,¹ Christophe Clanet,¹ and Michael Benzaquen¹

¹LadHyX, CNRS, Ecole Polytechnique, Institut Polytechnique de Paris, 91120 Palaiseau, France

(Dated: May 12, 2022)

Pumping at low Reynolds number is a ubiquitously encountered feature, both in biological organisms and engineered devices. Generating net flow requires the presence of an asymmetry in the system, which traditionally comes from geometric flow rectifiers. Here, we study a valveless system of N oscillating pumps in series, where the asymmetry comes not from the geometry but from time, that is the phase shifts between the pumps. Experimental and theoretical results are in very good agreement. We provide the optimal phase shifts leading to the maximal net flow in the continuous $N \rightarrow \infty$ limit, larger by 25% than that of a traditional peristaltic sinusoidal wave. Our results pave the way for the design of more efficient microfluidic pumps.

Pumping at low Reynolds number is a broadly encountered feature, both in nature and engineered systems. On the biological side, insects such as butterflies and mosquitoes feed essentially on liquids such as plant nectar or blood, and many rely on the action of one or more muscular pumps to intake their food [1]. On the man-made side, the design of micropumps for MEMS applications started with the seminal work of Smits 30 years ago [2], and continued with the Quake-valves now ubiquitous in microfluidic designs [3], triggering a large variety of novel designs [4–7].

In one way or another, these natural and engineered devices rely on the presence of an asymmetry in the system, which is essential to pump at low Reynolds number. Some biological and man-made pump designs rely on valves, a role played by the pharynx in mosquitoes [8–10]. Yet, valves are prone to mechanical failure and clogging, and valveless systems of micropumps were conceived to make them easier to fabricate and more resilient [5, 11]. Their mode of operation relies on geometrically asymmetric elements having flow-rectifying properties. Valveless pumping at low Reynolds number is also prevalent in biology, throughout the animal kingdom: in the early stages of embryonic development of a number of species, the heart consists in two chambers that pump fluid without a valve [12–14].

In this communication we study experimentally and theoretically a valveless pumping system consisting of N identical contracting pumps in series, operating at low Reynolds number. The system does not contain any flow rectifier (valveless), and the asymmetry comes not from the built-in geometry but from the phase shifts between the oscillating pumps, i.e. from the dynamics of actuation. The average flow rate through the system is computed from the system geometry and the phases of the oscillating pumps. Theoretical results are in very good agreement with experiments. We find numerically the phase shifts between the N pumps leading to maximal flow rate, for arbitrary values of N . When the number of pumps is increased to infinity (continuous limit), the maximum flow rate obtained is larger by 25% than that of a traditional peristaltic, sinusoidal wave. Our results

thereby cut the first turf for more efficient designs of microfluidic pumps.

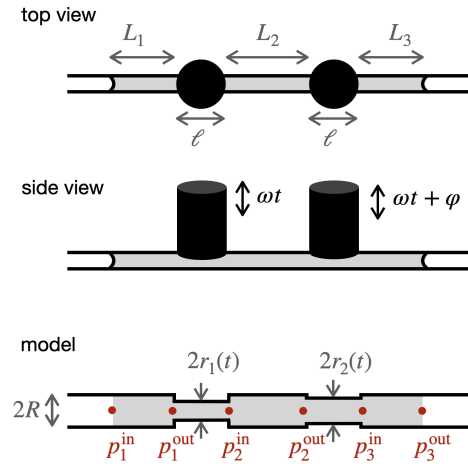


FIG. 1. Sketch of the experimental setup: two cylindrical wooden rods of diameter 1 cm placed on computer-controlled syringe pumps are used to press periodically on an elastic silicone tubing. The tubing is partially filled with V1000 silicon oil (gray). The parameterization of the system is as follows: two pumps of length ℓ delimit sections of a tubing of total length $L_{\text{tot}} = 2\ell + L_1 + L_2 + L_3$. The tubing radius is $R = 0.75$ mm. The varying tubing radius under the pumps is denoted $r_{1,2}(t)$.

Two pumps The experimental setup consists in a silicon tubing of internal diameter $2R = 1.5$ mm (Thermo Scientific TM Sterilin, Thermo Fischer, France), partially filled with silicon oil (Rhodorsil[®] 47V1000). Cylindrical wooden rods of diameter 1 cm are placed on computer-controlled syringe pumps (Nemesys, Cetoni GmbH, Germany), and press periodically on the silicon tubing, see Fig. 1. These wooden rods constitute the pumps. The evolution of the tubing diameter at the location of rod i can be approximated as $r_i(t) = R[1 - \varepsilon + \varepsilon \sin(\omega t + \varphi_i)]$, where ε is the normalized pumping amplitude, ω the pumping angular frequency and φ_i the phase shift of pump i , see Fig. 1. The column of oil of length L_{tot} is imaged at 10 Hz with a CMOS camera (Lt225c, Tele-

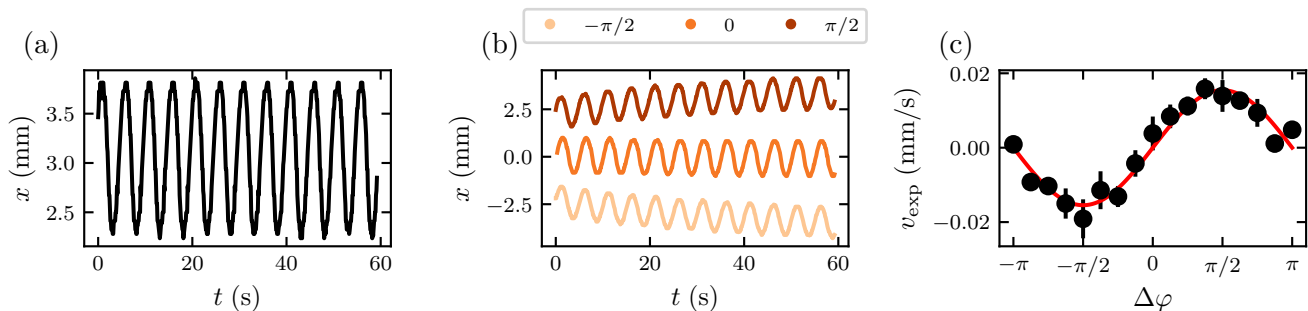


FIG. 2. (a) Oscillating position of the oil/air meniscus when one pump presses periodically on the silicone tubing, with a period $T = 5$ s. (b) When two pumps press periodically on the silicone tubing, the position of the meniscus shows a net drift superposed on oscillations at the forcing period. The drift direction depends on the sign of the phase shift $\Delta\varphi = \varphi_1 - \varphi_2$ between the two pumps. (c) Evolution of the mean drift speed v_{exp} as a function of the phase shift $\Delta\varphi$. Points: experimental data. Line: fit to a sine function.

dyne Lumenera, Canada), and the position of the oil/air interface is followed over time.

When only one pump is actuated, the oil/air meniscus moves periodically and symmetrically left and right at the forcing frequency, leading to on average zero net flow through the system, see Fig. 2a. This is typical of the reversible behavior of flows at low-Reynolds number: in the absence of inertia, a symmetric forcing on the fluid does not lead to any net flow [15]. The amplitude a of the oscillations enables us to estimate the normalized pumping amplitude $\varepsilon = 1 - \sqrt{1 - a/\ell}$, where $\ell = 1$ cm is the diameter of the wooden rod, and so the size of the pumping region (see the Supplementary Material for details).

When two pumps are actuated, the meniscus still moves periodically left and right at the forcing frequency, but in the presence of an additional, slower drift. The amplitude and direction of the drift depend on the phase shift $\Delta\varphi = \varphi_1 - \varphi_2$ between the two pumps, see Fig. 2b. The drift velocities of the meniscus are extracted from kymographs of the experiment, for all values of the phase shifts tested. The drift velocity v shows a sinusoidal dependency on the phase shift $\Delta\varphi$, see Fig. 2c, with no drift for $\Delta\varphi = 0, \pm\pi$, and a maximum drift for $\Delta\varphi = \pm\pi/2$. This can be intuitively understood by seeing that when the two pumps are in phase opposition ($\Delta\varphi = \pm\pi$), the fluid pushed by one pump fills up the space of the tube under the second pump, resulting in a reversible situation and so an absence of net flow. When the phase shift is $\Delta\varphi = \pm\pi/2$, the pump in phase retardation pushes the fluid preferentially away from the other pump, in a discretized version of peristaltic pumping.

Two pumps theory The flow generated by the pumps can be calculated under the assumption of small deformations $\varepsilon \ll 1$. Consider the valveless system of two

pumps pushing on a tubing of radius R and total length L_{tot} , as shown in Fig. 1. The pumps have a length ℓ , and the radius of the tubing at the location of the pumps is $r_i(t)$, $i = 1, 2$. The tubing is delimited by the pumps into three sections of length L_1 , L_2 and L_3 . The total length of the tubing is then $L_{\text{tot}} = L_1 + L_2 + L_3 + 2\ell$. The pressures at the inlet and outlet of the i -th section are $p_i^{\text{in}}(t)$ and $p_i^{\text{out}}(t)$, respectively (see bottom panel in Fig. 1). At low Reynolds numbers and in the cylindrical geometry presented here, flows obey Poiseuille's law, so that the flow rate $Q_i(t)$ in channel i is linked to the pressures $p_i^{\text{in}}(t)$ and $p_i^{\text{out}}(t)$ through:

$$\forall i \in [1, 3], \quad Q_i(t) = k_i [p_i^{\text{in}}(t) - p_i^{\text{out}}(t)], \quad (1)$$

where $k_i = \pi R^4 / 8\eta L_i$ is the resistivity of the channel. The flow rates between adjacent channels are related by mass conservation:

$$\forall i \in [1, 2], \quad Q_i(t) - Q_{i+1}(t) = 2\ell\pi r_i(t)\partial_t r_i. \quad (2)$$

Last, the flow in channel i can be expressed as a function of the resistivity $\kappa_i(t) = \pi r_i(t)^4 / 8\eta\ell$ of pump $i \in [1, 2]$:

$$Q_i(t) = \kappa_i(t)[p_i^{\text{out}}(t) - p_{i+1}^{\text{in}}(t)] + \ell\pi r_i(t)\partial_t r_i. \quad (3)$$

Equations (1)-(3) constitute a linear system of 7 scalar equations. The pressures are imposed to be identical at the inlet and outlet of the system: $p_1^{\text{in}} = p_3^{\text{out}} = p_0$. We solve for the 7 unknown variables $(Q_1, Q_2, Q_3, p_1^{\text{out}}, p_2^{\text{in}}, p_2^{\text{out}}, p_3^{\text{in}})$, looking for a solution to the equations when pumps are forced sinusoidally: $r_i(t) = R[1 - \varepsilon + \varepsilon \cos(\omega t + \varphi_i)]$.

The time-averaged flow $\bar{Q}_1 = \bar{Q}_2 = \bar{Q}_3 := \bar{Q}$ is found to depend on the phase difference $\Delta\varphi = \varphi_1 - \varphi_2$ between the two pumps through:

$$\bar{Q}(\Delta\varphi) = \frac{4\pi R^2 \ell^2 (L_{\text{tot}} - \ell - L_2)}{L_{\text{tot}}^2} \omega \varepsilon^2 \sin \Delta\varphi + \mathcal{O}(\varepsilon^3). \quad (4)$$

The average flow velocity $v_{\text{theor}, 2 \text{ pumps}} = \bar{Q}/\pi R^2$ in the tubing is then given by:

$$v_{\text{theor}, 2 \text{ pumps}} = 4(L_{\text{tot}} - \ell - L_2) \frac{\ell^2}{L_{\text{tot}}^2} \omega \varepsilon^2 \sin \Delta\varphi + \mathcal{O}(\varepsilon^3). \quad (5)$$

We recover the experimentally observed dependency of the flow speed on the sine of the phase difference $\sin \Delta\varphi$. The flow speed is proportional to the forcing frequency ω , as can be expected for low-Reynolds flows, and depends on a geometric prefactor that involves the ratio of the pump size ℓ to the total length of the fluid column L_{tot} : the larger the fraction of the fluid being pressed by the pumps, the more efficient the pumping. Note that $\ell = L_{\text{tot}}/2$ at most, for which the flow speed saturates to its maximum value. Last, note that pumping is a second-order effect in ε .

Experiments are repeated for different values of ε , L_{tot} and $\Delta\varphi$, and the experimental drift velocities of the oil are plotted as a function of the theoretical velocities in Fig. 3a. We find good agreement between the second-order theory and experiments for small values of $\varepsilon \lesssim 0.2$, and deviation from the second-order theory for higher values of ε , which results in the S-shape curve in Fig. 3a. Solving the equations of fluid motion up to order $\mathcal{O}(\varepsilon^3)$ and comparing the experiments to the third-order theory gives very good agreement for all parameters tested, up to a numerical prefactor, see Fig. 3b. The experimental speed is ≈ 3 times smaller than predicted by theory, see Fig. 3b. This can most likely be attributed to viscous dissipation in the meniscus [16]. The expression for the theoretical speed up to third order in ε is given in the Supplementary Material.

Three pumps The theory can be extended to a system of N pumps in series (see below). In particular, for a system of 3 identical pumps, and using the same notations as above, the average flow velocity is found to be:

$$v_{\text{theor}, 3 \text{ pumps}} = \frac{\ell^2}{L_{\text{tot}}^2} \omega \varepsilon^2 [a_1 \sin(\varphi_1 - \varphi_2) + a_2 \sin(\varphi_1 - \varphi_3) + a_3 \sin(\varphi_2 - \varphi_3)] + \mathcal{O}(\varepsilon^3), \quad (6)$$

where the a_i are geometrical prefactors that have the dimension of a length, and φ_i is the phase shift of pump i (see Supp. Mat. for the expressions of the a_i). The validity of this prediction is tested by mounting a system with 3 pumps, where the forcing amplitude ε , the length of the column of oil L_{tot} , and the phase shifts φ_1 and φ_2 are systematically varied. Experimental results are in very good agreement with theoretical predictions, up to a numerical prefactor, see Fig. 4. As for the system with two pumps, the experimental velocities for the three-pump device are smaller than theoretical predictions, again most likely due to viscous dissipation in the meniscus (see black dashed line in Fig. 4).

N pumps Is pumping more efficient when more pumps are added to the system? To answer this ques-

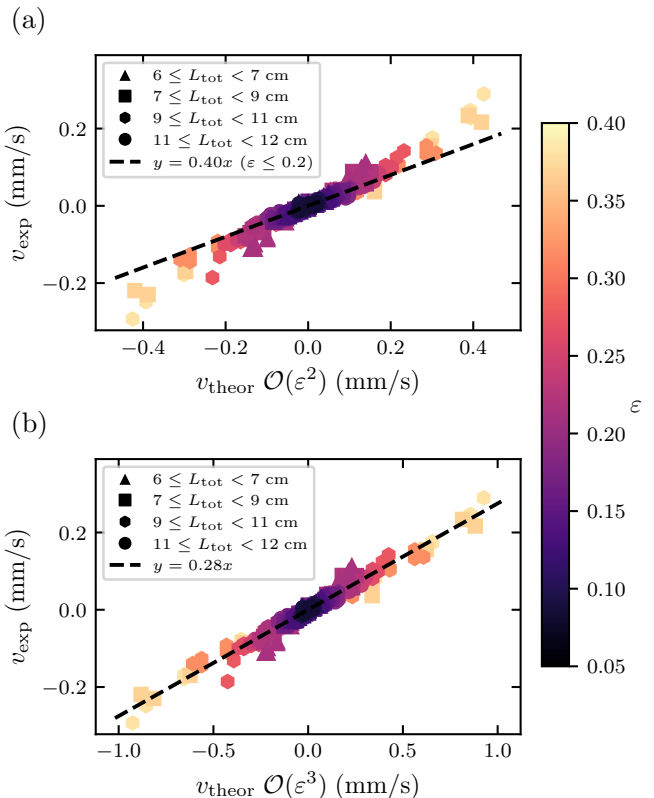


FIG. 3. Comparison between the experimental and theoretical flow speeds (points), for a system of two pumps. The normalized pumping amplitude ε is color-coded, different symbols are for different lengths of liquid column L_{tot} . Other parameters: $2R = 1.5$ mm, $\ell = 1$ cm, $L_2 = 3$ cm. (a) Experimental vs. theoretical speed calculated up to $\mathcal{O}(\varepsilon^2)$. The dashed line is the best fit to data with $\varepsilon \leq 0.2$. (b) Experimental vs. theoretical speed calculated up to $\mathcal{O}(\varepsilon^3)$. The dashed line is the best fit to all data.

tion, consider a system of N identical pumps of length ℓ in series, actuated sinusoidally. For simplicity, we now consider that all subsections of the tubing have the same length L , and so the same resistivity $k = \pi R^4/8\eta L$. The total length of the tubing is then $L_{\text{tot}} = N\ell + (N+1)L$. Similarly to Eq. (1)-(3), there are now $3N+1$ equations to solve in order to compute the flow rate:

$$\forall i \in [1, N+1], \quad Q_i(t) = k[p_i^{\text{in}}(t) - p_i^{\text{out}}(t)]. \quad (7a)$$

$$\forall i \in [1, N], \quad Q_i(t) - Q_{i+1}(t) = 2\ell\pi r_i(t)\partial_t r_i, \quad (7b)$$

$$Q_i(t) = \kappa_i(t)[p_i^{\text{out}}(t) - p_{i+1}^{\text{in}}(t)] + \ell\pi r_i(t)\partial_t r_i. \quad (7c)$$

The same pressure is imposed at the inlet and the outlet ($p_1^{\text{in}} = p_{N+1}^{\text{out}} = p_0$), and the system of equations is solved for the $3N+1$ unknown variables $(Q_1, \dots, Q_N, p_1^{\text{out}}, p_2^{\text{in}}, p_2^{\text{out}}, \dots, p_N^{\text{out}}, p_{N+1}^{\text{in}})$, when pumps are forced sinusoidally $r_i(t) = R[1 - \varepsilon + \varepsilon \sin(\omega t + \varphi_i)]$.

The average flow rate over one period T through a

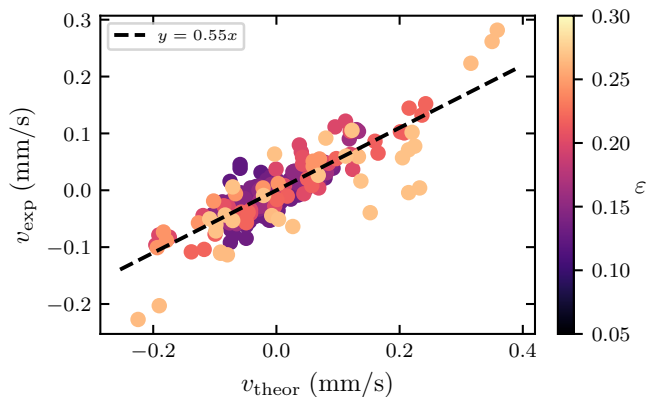


FIG. 4. Comparison between the more than 200 experimental flow speed values measured and the theoretical speed values (points), for a system of three pumps. The normalized pumping amplitude ε is color-coded. The liquid length L_{tot} was varied between 13 and 18 cm. Other parameters: $2R = 1.5$ mm, $l = 1$ cm. Theoretical speed calculated up to $\mathcal{O}(\varepsilon^2)$, according to Eq. (6). The dashed line is the best fit to all data.

system of N pumps is found to be:

$$\bar{Q}(\{\varphi_i\}) = 4\pi R^2 \ell \omega f_N(\varepsilon, b, \{\varphi_i\}) + \mathcal{O}(\varepsilon^3), \quad (8)$$

where we have introduced $b = \ell/L$, the ratio of the pump dimension to that of the tubing sections, and

$$f_N(\varepsilon, b, \{\varphi_i\}) = \frac{b}{(Nb + N + 1)^2} \times \left(\sum_{M=1}^{N-1} (M(b+1) + 1) \sum_{i=1}^M \sin(\varphi_i - \varphi_{i+N-M}) \right) \varepsilon^2 + \mathcal{O}(\varepsilon^3). \quad (9)$$

The flow rate therefore depends on the phase shifts between the pumps, and on the aspect ratio $b = \ell/L$; it increases linearly with b for small b and saturates for $b \gg 1$, when the pumps essentially press on the entire length of the tubing.

The phase shifts giving the maximal flow rate for a given aspect ratio b were obtained numerically. For the particular case of $N = 2$ pumps, the maximum flow rate is obtained for $\Delta\varphi = \pm\pi/2$, independent of the aspect ratio b . For $N > 2$ pumps, the combination of phase shifts leading to the maximum flow rate depends slightly on the aspect ratio b . For a system of $N \geq 3$ pumps, the optimal phase shifts depend on the aspect ratio b , albeit only weakly (for $N = 3$ pumps, varying b over 10 orders of magnitude changes the optimal values of the phase shifts by $\approx 5\%$). Actually, for all tested values of $N \geq 3$, the optimal phases shifts are essentially constant for $b \ll 1$ and $b \gg 1$, and undergo a small variation when the aspect ratio b goes from 0.1 to 10.

Because the energy needed to actuate N pumps increases linearly with N , to compare the efficiency of

pumping as a function of the number of pumps, it is necessary to impose a forcing that depends on N : $\tilde{r}_i(t) = R[1 - \varepsilon/\sqrt{N} + \varepsilon/\sqrt{N} \sin(\omega t + \varphi_i)]$. Such a forcing ensures that the total energy spent is the same for all systems of pumps. The flow rate in the system is then simply given by $\bar{Q}(\{\varphi_i\}) = \tilde{Q}(\{\varphi_i\})/N$.

The maximal flow rate in the system $\tilde{Q}_{\text{max}}(N)$ increases with the number of pumps N until saturation in the continuous limit ($N \rightarrow \infty$), see black markers in Fig. 5a. The maximal flow rate in a system of 2 pumps is $\approx 60\%$ as large as in the continuous limit. The increase in flow rate is very steep when N initially increases: the flow rate in a system of 3 pumps is already $\approx 80\%$ that of the continuous limit, and 5 pumps guarantee a flow rate of $\approx 90\%$ that of the continuous system.

Regardless of the number of pumps N in the system, the optimal flow rate \tilde{Q}_{max} is always larger than the flow rate \tilde{Q}_{sine} obtained by naively discretizing a sine wave, for which the phase shifts are equally spaced by $2\pi/N$ (see the orange markers in Fig. 5a, and the dashed orange line in Fig. 5b). This is most obvious for $N = 2$, where discretizing a sine wave leads to the two pumps being actuated in phase opposition, which does not induce any net flow. For $N = 3$ pumps, the optimal flow rate is $\approx 65\%$ larger than \tilde{Q}_{sine} (see inset in Fig. 5a). The ratio $\tilde{Q}_{\text{max}}/\tilde{Q}_{\text{sine}}$ decreases when N increases, and in the continuous limit, the optimal flow rate is 25% larger than the flow rate obtained with a sinusoidal peristaltic wave, see the difference between black and orange points in Fig. 5a and inset in Fig. 5a.

The waveform leading to the maximal flow rate in the continuous limit is shown in black in Fig. 5b for large N , at time $t = 0$. This optimal wave travels along the tube over one period of oscillation. The optimal waveform is different from the traditional sinusoidal peristaltic wave in two striking ways. First, the optimal wave is asymmetric. Second, the phase values of the first and last pumps are strikingly different, leading to a sharp discontinuity that travels over the tube over one period of oscillation.

Discussion The literature on miniaturized pumps, which operate at low Reynolds number, is extremely vast, and covers aspects from fluid dispensing in lab-on-a-chip devices for biological analysis [17] to biomedical applications such as microdosing for drug delivery [7]. Yet, the broad majority of the existing work is concerned with the flow generated by at least 3 pumps in series, with very few exceptions on pumping with two pumps [18–20]. To the best of our knowledge, and to the notable exception of the work by Goulpeau et al. [21] who modelled a system with 3 pumps, no physical model of the flow generated by these discrete pumps exists for an arbitrary number of pumps. On the same vein, we have found no work on the influence of the geometric parameters of the fluidic circuit, or of the phase shifts between the pumps, on the flow rate, for arbitrary number of pumps.

To achieve the highest flow rate possible, existing work

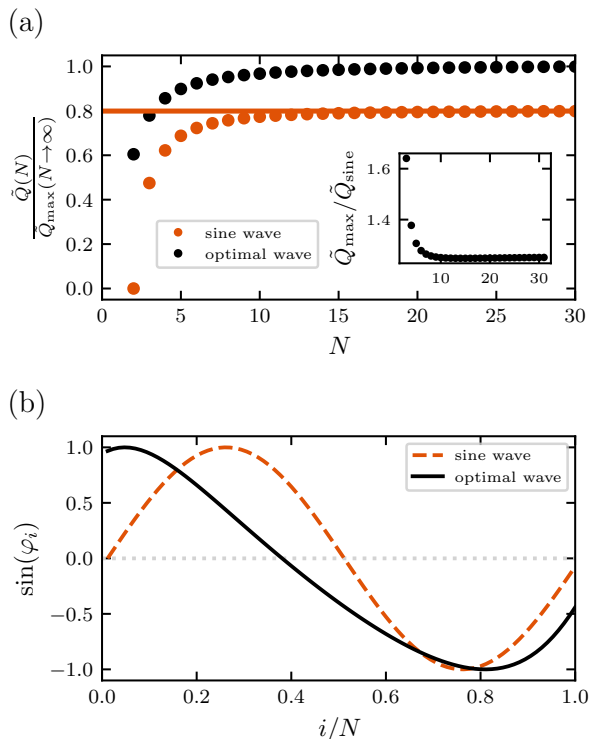


FIG. 5. (a) For a given input energy, increasing the number of pumps in the system increases the optimal flow rate $\tilde{Q}_{\max}(N)$ (black dots), up to a limit corresponding to the continuous case $N \rightarrow \infty$. The optimal flow rate is always larger than the flow rate obtained by naively discretizing a sine wave, where the phase shifts are equally spaced by $2\pi/N$ (orange dots). Inset: ratio between the optimal flow rate $\tilde{Q}_{\max}(N)$, and the flow rate $\tilde{Q}_{\text{sine}}(N)$ obtained by discretizing a sine wave, as a function of N . (b) Waveform leading to the maximum flow in a system of N pumps with $N = 30$. Increasing N further does not change the waveform.

usually sets the phase shifts to arbitrary, intuitive values, and then measures the flow rate as a function of the frequency of actuation of the pumps, see e.g. [20, 22–25]. At low Reynolds number however, both quantities are proportional; deviation from proportionality indicates either a change of regime to high Reynolds number, or reveals the presence of a compliance in the microsystem, which induces a phase shift between the applied actuation signal and the real mechanical actuation. This difference between the applied actuation and the real actuation is probably at the origin of surprising results, such as obtaining a maximum flow rate in a system of two pumps when they are supposedly actuated in phase ($\Delta\varphi = 0$) or in phase opposition ($\Delta\varphi = \pi$) [20], in direct contradiction with the reversibility of flows at low Reynolds number. Our results show that, in the low Reynolds regime, valveless pumping with two pumps is optimal for phase shifts between the pumps $\Delta\varphi = \pm\pi/2$, and we provide

the exact analytical expression of pumping efficiency as a function of the geometric parameters of the problem. Theoretical and experimental results are in good agreement, see Figs. 3 and 4.

The flow due to a simple peristaltic wave travelling along a tube can be analytically calculated, see [26, 27], with a number of applications. Original ideas making use of peristaltic waves were put forth, e.g. for the swimming of microorganisms [28, 29]. The optimization of peristaltic wave shapes at low Reynolds number has been studied numerically using variational methods [30] and, more recently, boundary integral methods [31]. Here, we obtained numerical results on the optimal peristaltic wave shape at low Reynolds number by studying a system of N discrete pumps, and let $N \rightarrow \infty$, see Fig. 5. The non-trivial optimal peristaltic shape we find leads to a flow rate larger by 25% than that due to a sinusoidal peristaltic wave. Moreover, in the discrete case of a small number of pumps, the difference between the optimal flow rate and the flow rate obtained by naively discretizing a sine wave is even larger: for $N = 3$ pumps, the optimal flow rate is $\approx 65\%$ larger than that obtained with a discretized sine wave.

Finally, note that the results presented here are valid for a system of N pumps actuated independently of each other, in a regime where the imposed actuation is instantaneously transmitted to the fluid. They do not take into account effects due to the elasticity of the tubing enclosing the fluid. Elasticity introduces a compliance in the system as mentioned above, and can also lead to two neighboring pumps not being independent of each other: if the pumps are too close to each other, closing one pump will open the neighboring one. The analysis of such intricate effects is left for future work.

Acknowledgments We thank Roméo Antier for his contribution to the early stages of this work, and Caroline Frot for her valuable help with fabrication.

-
- [1] B. J. Borrell and H. W. Krenn, in *Ecology and Biomechanics: A Mechanical Approach to the Ecology of Animals and Plants*, edited by A. Herrel, T. Speck, and N. P. Rowe (CRC Press, 2006) Chap. 9, pp. 185 – 212.
 - [2] J. G. Smits, *Sensors and Actuators: A. Physical* **21**, 203 (1990).
 - [3] M. a. Unger, H. P. Chou, T. Thorsen, a. Scherer, and S. R. Quake, *Science (New York, N.Y.)* **288**, 113 (2000).
 - [4] D. J. Laser and J. G. Santiago, *Journal of Micromechanics and Microengineering* **14**, R35 (2004).
 - [5] P. Woias, *Sensors and Actuators B: Chemical* **105**, 28 (2005).
 - [6] B. D. Iverson and S. V. Garimella, *Microfluidics and Nanofluidics* **5**, 145 (2008).
 - [7] A. B. Bußmann, L. M. Grünerbel, C. P. Durasiewicz, T. A. Thalhofer, A. Wille, and M. Richter, *Sensors and Actuators, A: Physical* **330**, (2021).

- [8] K. Uchida, *International Journal of Insect Morphology and Embryology* **8**, 159 (1979).
- [9] B. H. Kim, E. S. Seo, J. H. Lim, and S. J. Lee, *Microscopy Research and Technique* **75**, 1051 (2012).
- [10] K. Kikuchi, M. A. Stremmler, S. Chatterjee, W. K. Lee, O. Mochizuki, and J. J. Socha, *Scientific Reports* **8**, 1 (2018).
- [11] E. Stemme and G. Stemme, *Sensors and Actuators: A. Physical* **39**, 159 (1993).
- [12] N. S. Glickman and D. Yelon, in *Seminars in cell & developmental biology*, Vol. 13 (Elsevier, 2002) pp. 507–513.
- [13] E. N. Olson, *Science* **313**, 1922 (2006).
- [14] P. J. Scherz, J. Huisken, P. Sahai-Hernandez, and D. Y. Stainier, *Development* **135**, 1179 (2008).
- [15] E. E. Purcell, *American Journal of Physics* **45**, 11 (1977), arXiv:arXiv:1011.1669v3.
- [16] A back-of-the-envelope calculation gives similar orders of magnitude for injected energy and viscous dissipation in the meniscus, consistent with the present discrepancy.
- [17] Y. N. Wang and L. M. Fu, *Microelectronic Engineering* **195**, 121 (2018).
- [18] J. M. Berg, R. Anderson, M. Anaya, B. Lahlouh, M. Holtz, and T. Dallas, *Sensors and Actuators, A: Physical* **104**, 6 (2003).
- [19] A. Geipel, A. Doll, P. Jantschkeff, N. Esser, U. Massing, P. Woias, and F. Goldschmidtboeing, *Journal of Micromechanics and Microengineering* **17**, 949 (2007).
- [20] B. H. Kim, I. C. Kim, Y. J. Kang, J. Ryu, and S. J. Lee, *Sensors and Actuators A: Physical* **209**, 133 (2014).
- [21] J. Goulpeau, D. Trouchet, A. Ajdari, and P. Tabeling, *Journal of Applied Physics* **98**, 10.1063/1.1947893 (2005).
- [22] J. Xie, J. Shih, Q. Lin, B. Yang, and Y. C. Tai, *Lab on a Chip* **4**, 495 (2004).
- [23] L. S. Jang and W. H. Kan, *Biomedical Microdevices* **9**, 619 (2007).
- [24] G. Liu, C. Shen, Z. Yang, X. Cai, and H. Zhang, *Sensors and Actuators, A: Physical* **163**, 291 (2010).
- [25] O. Fuchs, Y. Fouillet, S. Maubert, M. Cochet, C. Chabrol, N. David, X. Médal, and R. Campagnolo, *Microelectronic Engineering* **97**, 375 (2012).
- [26] A. Shapiro, M. Jaffrin, and S. Weinberg, *J. Fluid Mech* **37**, 799 (1969).
- [27] M. Y. Jaffrin and a. H. Shapiro, *Annual Review of Fluid Mechanics* **3**, 13 (1971).
- [28] A. Ajdari, P.-G. De Gennes, J.-P. Hulin, L. Leibler, and J. Prost, *Comptes rendus de l'Académie des sciences. Série II, Mécanique, physique, chimie, astronomie* **319**, 861 (1994).
- [29] A. Ajdari and H. A. Stone, *Physics of Fluids* **11**, 1275 (1999).
- [30] S. W. Walker and M. J. Shelley, *Journal of Computational Physics* **229**, 1260 (2010).
- [31] M. Bonnet, R. Liu, and S. Veerapaneni, *Advances in Computational Mathematics* **46**, 1 (2020).